Further Validation of the Global Human Body Model Consortium 50th Percentile Male Pelvis Finite Element Model

Daniel Grindle, Yunzhu Meng, Costin Untaroiu

Virginia Tech

Abstract

Road traffic accidents are the eighth leading cause of death worldwide, killing 1.35 million annually. The Global Human Body Model Consortium (GHBMC) has previously created and validated a finite element model of a 50th percentile male pedestrian in LS-DYNA® to investigate vehicle-pedestrian impacts. To assure and improve the model's biofidelity, additional model improvements were made to the GHBMC pelvis model. These pelvis developments included the addition of acetabular cartilage and the optimization of material properties. The updated pelvis model was calibrated against Post-Mortem Human Surrogate (PMHS) component tests: dynamic lateral acetabulum loading, dynamic lateral iliac wing loading, and quasi-static sacroiliac joint loading. After new material properties were established for the pelvis model, the updated properties were applied to the whole-body GHBMC model. The updated model pelvis injury response was validated against whole-body PMHS lateral vehicle impact tests. More biofidelic biomechanical responses were observed in the updated pelvis model in the majority of component level validations. In addition, the fracture patterns of the updated pelvis matched the PMHS fracture patterns in whole-body impacts. This updated pelvis model will be incorporated into the next generation of GHBMC models. In future, it can be used to properly investigate pelvis injury mechanisms in impact scenarios to reduce pedestrian injuries in traffic accidents.

Introduction

Road traffic crashes are the eighth leading cause of the death worldwide, killing about 1.35 million people per year [1]. Between 2008 and 2018, the United States experienced a 6% decrease in occupant traffic fatalities but a 41% increase in pedestrian fatalities in Car-to-Pedestrian-Collisions (CPCs) [2]. In CPC accidents, pedestrian lower extremity injuries are common, accounting for 31.2% of CPC injuries. These lower extremity injuries may not directly lead to death, but can cause life-long disabilities. This increase in injuries and fatalities has led to an increased level of new vehicle safety testing.

New vehicle pedestrian safety evaluations typically use isolated body components to investigate the potential injuries a pedestrian may experience in vehicle impacts [4-7]. Subsystem impact tests provide some insight but cannot capture the complex whole-body pedestrian-vehicle interaction critical to investigating pedestrian injury mechanics. To capture the whole-body pedestrian-vehicle interaction, finite element (FE) models of the human body have been developed and used to simulate vehicle impacts.

The Global Human Body Model Consortium (GHBMC) has created a FE model of a male pedestrian, in LS-DYNA, whose anthropometry closely matches the 50th percentile North American male [8]. The model has been validated at the regional level [9-19] and the whole-body level [20-25] in vehicle impact scenarios. In impact scenarios, the lower extremity is susceptible to injury. The main objective of this study was to evaluate the biofidelity of the GHBMC model's pelvis components in impact experiments, and if we could improve the model responses by altering model material properties.

Methods

Development and Validation of the GHBMC Finite Element Pelvis

The GHBMC pelvis model consists of the ilium, sacrum, sacroiliac joint cartilage and ligaments, and pubic symphysis joint cartilage (Figure 1). The whole pelvis model has 64,828 nodes and 198,293 deformable elements (704 shells, 32 beams, 197521 solid) and all parts of the model were connected using shared nodes and/or tied node interfaces. The geometry of the pelvis was collected using a multi-modality approach [26] from a volunteer whose anthropometry closely matched the 50ᵗʰ percentile North American male [8, 27]. The initial material properties of the GHBMC pelvis model were taken from various PMHS studies, literature reviews, and modeling studies [28-30]. All of the pelvis model material properties are taken from literature, except the properties of the sacroiliac joint (SIJ). The SIJ was not assigned literature-based material properties because they have not been established in literature.

The cartilage geometry was modeled to match medical illustrations from Grey's Anatomy, and the cartilage thickness was determined by taking a reasonable value from literature [31, 32]. The material properties of the cartilage were assigned to be the same as the original SIJ cartilage, a Mooney-Rivlin rubber.
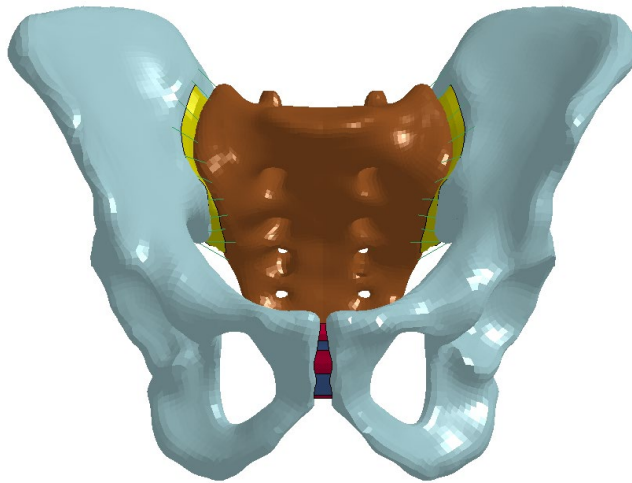

Figure 1. GHBMC pelvis model rendered in LS-PrePost®

Dynamic Lateral Pelvis Loading

The pelvis model was validated against two dynamic lateral loading tests which created loading conditions similar to a lateral vehicle impact [33]. The non-impacted side of the pelvis was cut through the ilium and the superior and inferior components were constrained in separate pots which were free to move superior-inferior to the pelvis. To apply load to the pelvis, a 76.6 kg drop impactor impacted a transfer beam which then loaded a surface that contacted the pelvis. The pelvis was impacted in two separate scenarios.

The first loading scenario transferred the drop tower load to a metallic ball located at the acetabulum, the second loading scenario transferred load to a foam plate located at the iliac wing. The impactors were free to move anterior-posterior to the pelvis to replicate a realistic impact. The force transmission distributed through the anterior and posterior pelvis paths were recorded and reaction force-impactor displacement corridors were established for the acetabulum and iliac wing impacts [34]. Force-displacement response data was used after reaction forces reached 100 N in the acetabulum impact or 500 N in the iliac wing impact and force-deflection corridors were developed as one standard deviation above and below the average force-displacement response.

The two dynamic lateral loading scenarios were replicated in-silico using the GHBMC pelvis model. Velocity-time curves of the impactors from the PMHS experiments were applied to a sphere and a rigid plate connected to foam as boundary conditions [35]. The acetabulum impactor was modeled as a rigid body sphere and the iliac wing impactor was modeled as a rigid plate connected to CF-45 Confor Foam (EAR Speciality Composites, Indinaapolis) [36]. The two impact simulations were run twice, once with the original GHBMC pelvis model, and once with the addition of acetabulum cartilage and altered pelvis bone material parameters. The newly established material properties for bone were within the values reported in literature.
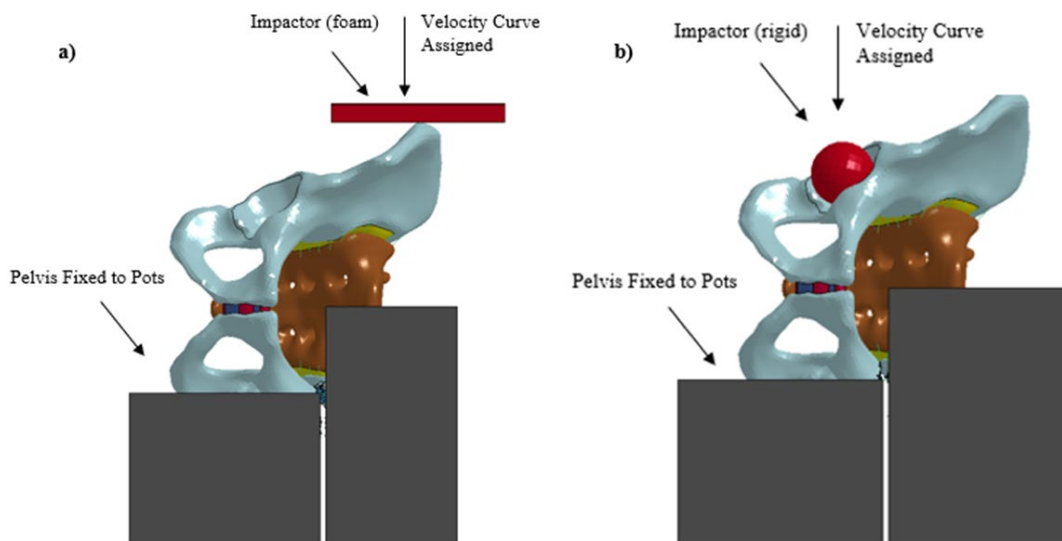

Figure 2. Dynamic lateral pelvis loading test setup at a) acetabulum b) iliac wing

Quasi-static Pelvis Loading of Sacroiliac Joint

The pelvis model's SIJ material properties were optimized in 5 quasi-static loading tests. In the quasi-static PMHS tests the posterior vertebral elements of the sacrum were removed, the coxal ends of the SIJ were fixed to a rigid test apparatus, and unidirectionally loads were applied to the sacrum between the S1 and S2 vertebral plates. The SIJ was loaded with 294 N in the anterior, posterior, superior, inferior, and mediolateral directions individually. The center of the superior S1 endplate was used to measure displacement [37]. To replicate this experiment in-silico, the GHBMC pelvis was set up in accordance with the PMHS test, allowing only SIJ stretching and sacrum displacement. 294 N point loads were applied to a single node on the anterior and posterior surface of the sacrum, lying mid-sagittal and between the S1 and S2 end plates in accordance with the PMHS test (Figure 3). A node on the center of the superior sacral endplate was chosen as the reference point to measure displacement. In 5 separate simulations the point loads were applied in the anterior, posterior, superior, inferior and mediolateral direction.   These simulations were completed twice, first with the original GHBMC SIJ, then with an optimized SIJ which incorporated the updated bone material properties established from the dynamic lateral loading simulations.
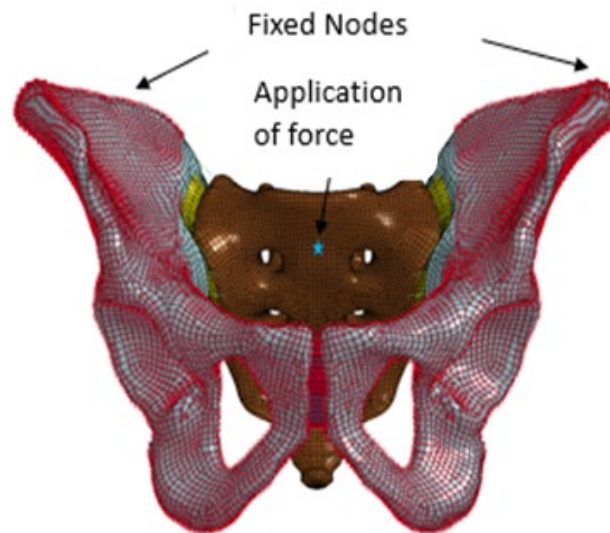

Figure 3. Quasi-static sacroiliac joint displacement test set-up

The GHBMC SIJ material properties were optimized using LS-OPT® software. The material properties chosen to optimize were the two Mooney-Rivlin constants and the Young's modulus of the SIJ cartilage and ligaments respectively. The material properties were optimized using Space Filling procedures and a Radial Basis Function Network metamodel. Properties were continuously sampled between +50% and -50% of their original starting values. The first Mooney-Rivlin constant was set to zero in the original GHBMC pelvis model, but was set to 0.0001 in this optimization in order to follow the continuous sampling procedure. The material properties were optimized to the quasi-static anterior, posterior, superior, inferior loadings, and the dynamic lateral loading at the iliac wing. Dynamic lateral loading at the acetabulum was not sensitive to SIJ soft tissue material parameters, thus it was removed from the optimization to reduce computational costs. The updated bone material properties established in the dynamic lateral impact simulations were incorporated into the pelvis model for the SIJ optimization.

Whole Body Impact Pelvis Injury Response

After new pelvis material properties were assigned from the quasi-static and dynamic loading simulations, the updated GHBMC pelvis injury response was validated against PMHS testing in full body impacts [38]. PMHS whose anthropometry corresponded to the 50ᵗʰ percentile male, were laterally impacted at 40 km/h by three generic vehicle bucks representing the sedan, SUV, and van. The PMHS were positioned in mid-gait stance with their arms tied in front of them, and were laterally impacted at the vehicle centerlines. To replicate these vehicle impacts in-silico, the GHBMC whole body model was impacted at 40 km/h by FE models of the three generic vehicle bucks using the same PMHS positioning protocols (Figure 4). GHBMC injury outcomes were compared to PMHS testing to check model biofidelity.
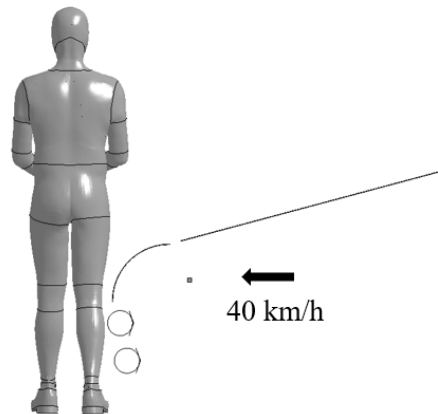

Figure 4. GHBMC whole body model with simplified sedan buck

Results

The GHBMC pelvis material parameters were altered to fit dynamic lateral acetabulum loading tests and optimized to fit both quasi-static SIJ loading dynamic lateral iliac wing loading tests. The new established material properties were within values found in literature (Table 1) [28, 35, 39]. The updated GHBMC pelvis produced more biofidelic responses than the original pelvis in all but one PMHS component test.

Table 1. Original and updated pelvis material properties.

Part	LS-DYNA Material Model	Original Properties	Updated Properties
Sacrum Cortical Bone	Plastic Kinematic	$\rho = 1.6E-6$ $E = 17$ $Pr = 0.29$ $\sigma_y = 0.085$ $E_{Tan} = 1.7$ $\beta_{Harden} = 0.1$	$\rho = 1.6E-6$ $E = 12\,0$ $Pr = 0.29$ $\sigma_y = 0.085$ $E_{Tan} = 1.2$ $\beta_{Harden} = 0.1$
Sacrum Trabecular Bone	Plastic Kinematic	$\rho = 1.2E-6$ $E = 0.07$ $Pr = 0.2$ $\sigma_y = 0.0092$ $E_{Tan} = 0.007$ $\beta_{Harden} = 0.1$	$\rho = 1.2E-6$ $E = 0.055$ $Pr = 0.2$ $\sigma_y = 0.0092$ $E_{Tan} = 0.0055$ $\beta_{Harden} = 0.1$
Coxal Cortical Bone	Plastic Kinematic	$\rho = 1.6E-6$ $E = 11.35$ $Pr = 0.29$ $\sigma_y = 0.085$ $E_{Tan} = 1.7$ $\beta_{Harden} = 0.1$	$\rho = 1.6E-6$ $E = 11.35$ $Pr = 0.29$ $\sigma_y = 0.085$ $E_{Tan} = 1.135$ $\beta_{Harden} = 0.1$
Coxal Trabecular Bone	Plastic Kinematic	$\rho = 1.2E-6$ $E = 0.07$ $Pr = 0.2$ $\sigma_y = 0.0092$ $E_{Tan} = 0.007$ $\beta_{Harden} = 0.1$	$\rho = 1.2E-6$ $E = 0.055$ $Pr = 0.2$ $\sigma_y = 0.0092$ $E_{Tan} = 0.0055$ $\beta_{Harden} = 0.1$
Sacroiliac Joint Cartilage	Mooney-Rivlin Rubber	$\rho = 1.2E-6$ $Pr = 0.495$ $a = 0$ $b = 0.0041$	$\rho = 1.2E-6$ $Pr = 0.495$ $a = 1E-4$ $b = 1E-3$
Sacroiliac Joint Ligament	Cable Discrete Beam	$\rho = 1.2E-6$ $E = 0.25$	$\rho = 1.2E-6$ $E = 0.01$
Pubis Symphysis Joint	Hyperelastic Rubber	$\rho = 1.2E-6$ $Pr = 0.495$ $C_{10} = 5E-5$ $C_{01} = 2E-4$ $C_{11} = 2.5E-4$ $G_{Relaxation} = 1.5E-5$ $\beta_{Decay} = 0.54$	$\rho = 1.2E-6$ $Pr = 0.495$ $C_{10} = 5E-5$ $C_{01} = 2E-4$ $C_{11} = 2.5E-4$ $G_{Relaxation} = 1.5E-5$ $\beta_{Decay} = 0.54$
	Soft Tissue Viscoelastic	$\rho = 1.2E-6$ $C_1 = 1.44E-3$ $C_2 = 0$ $C_3 = 1.9E-4$ $C_4 = 35.5$ $C_5 = 0.155$ $K = 1.44$ Stretch Ratio $= 1.055$ Spectral Strength$_1 = 9.2E-5$ Specrtal Strength$_2 = 4.03E-4$ Characteristic Time$_1 = 1.85$ Characteristic Time$_2 = 16.72$	$\rho = 1.2E-6$ $C_1 = 1.44E-3$ $C_2 = 0$ $C_3 = 1.9E-4$ $C_4 = 35.5$ $C_5 = 0.155$ $K = 1.44$ Stretch Ratio $= 1.055$ Spectral Strength$_1 = 9.2E-5$ Specrtal Strength$_2 = 4.03E-4$ Characteristic Time$_1 = 1.85$ Characteristic Time$_2 = 16.72$
Acetabulum Cartilage	Mooney-Rivlin Rubber	Did not exist in original model	$\rho = 1.2E-6$ $Pr = 0.495$ $a = 0$ $b = 0.0041$

Dynamic Lateral Pelvis Loading

In the dynamic lateral acetabulum loading simulation the updated GHBMC pelvis anterior and posterior responses were with-in the test corridor longer than the original pelvis model (Figure 5). In the dynamic lateral iliac wing loading the updated pelvis responses varied between anterior and posterior. The updated pelvis posterior response performed drastically better than the original pelvis, lying within the corridors for the entire simulation (Figure 6). In contrast, the updated pelvis anterior response performed slightly worse than the original pelvis, lying in the corridor for a small period of time.
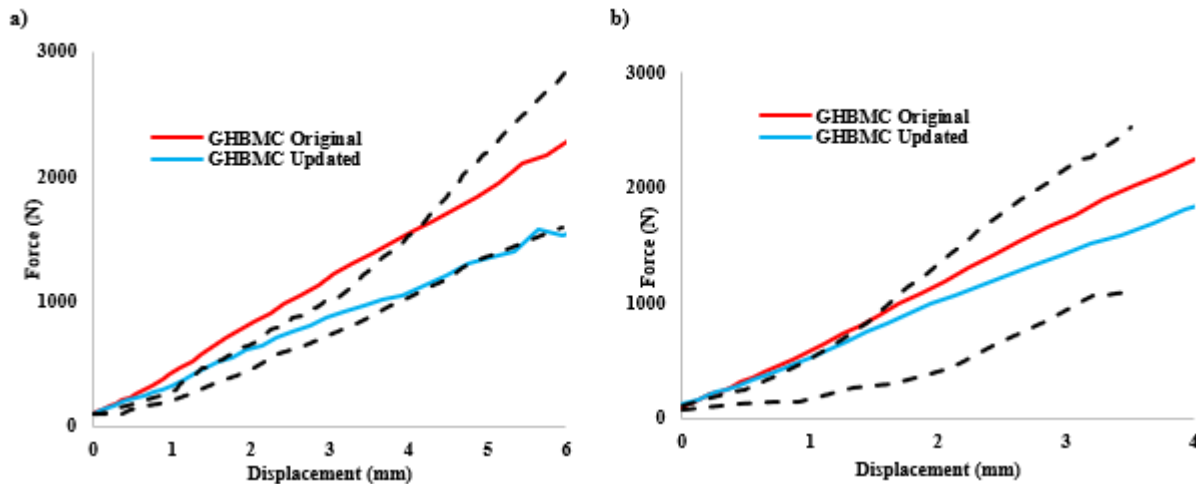
Figure 5. Dynamic lateral acetabulum loading a) posterior b) anterior force responses for original and updated GHBMC models against test corridors
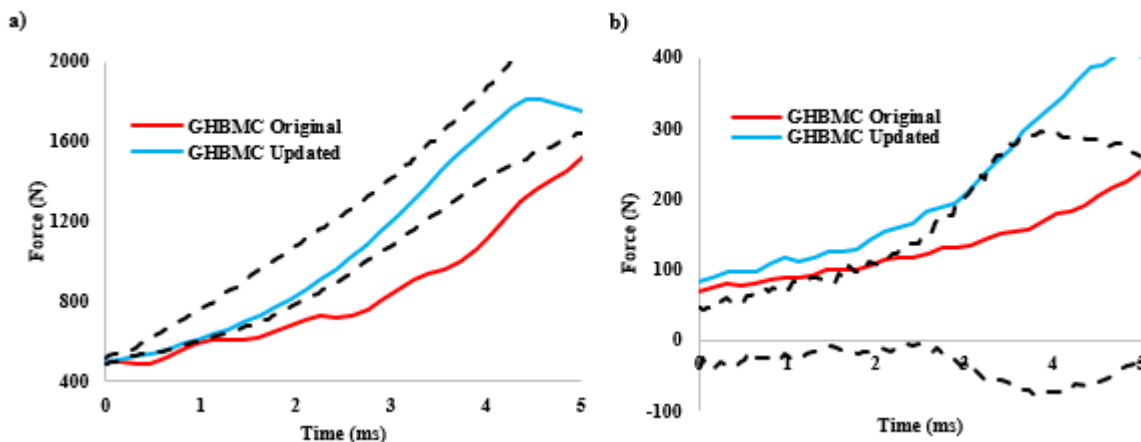
Figure 6. Dynamic lateral iliac wing loading a) posterior b) anterior force responses for original and updated GHBMC models against test corridors

Quasi-static Pelvis Loading of Sacroiliac Joint

In the SIJ quasi-static loading tests, loads were individually applied to in the superior, inferior, anterior, posterior, and medio-lateral directions. The updated GHBMC pelvis model responded within one standard deviation of the PMHS data in all five loading cases (Figure 7). In contrast, the original GHBMC pelvis model response was within one standard deviation for only three loading cases.
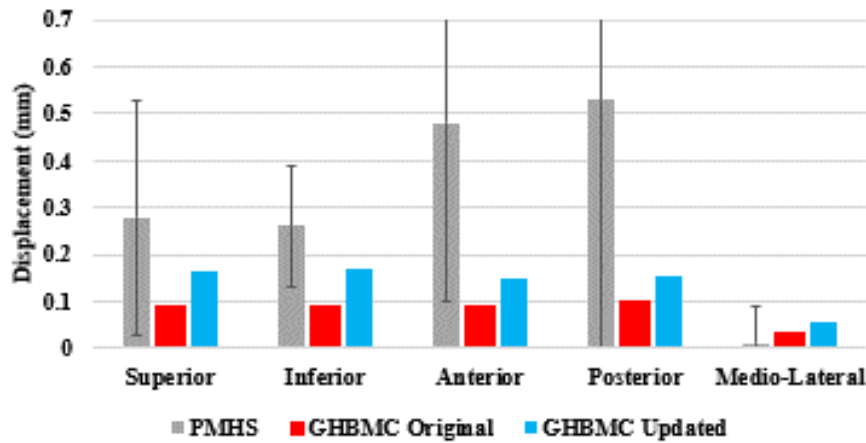

Figure 7. Quasi-static sacroiliac joint loading displacement response for PMHS, original GHBMC model, and updated GHBMC model.

Whole Body Impact Pelvis Injury Response

In the whole body PMHS and GHBMC lateral impacts, impact side pelvis injury outcomes were recorded and compared (Table 2). The PMHS and GHBMC model reported similar fractures for all three vehicle impacts.

In the sedan impact the only fracture reported was in one PMHS where the sacral ala was fractured. The GHBMC model did not experience a sacral ala fracture, but besides this instance neither the GHBMC model nor the PMHS experienced pelvis fractures on the impacted side.

The SUV impact response matched well between PMHS and GHBMC model. The GHBMC model and the majority of PMHS experienced sacral ala, inferior and superior pubic rami fractures. The GHBMC model and a minority of PMHS experienced acetabulum fractures. One PMHS iliac wing fractured and the GHBMC model iliac wing did not.

The van impact responses matched well between PMHS and the GHBMC model. The GHBMC model and the majority of PMHS experienced sacral ala, superior and inferior pubic rami, and acetabulum fractures. Neither the GHBMC model nor any of the PMHS experienced iliac wing fractures.

Table 2. Impact fracture responses of PMHS and updated GHBMC model in three lateral impact scenarios.

Impacted Side: Body Component	Sedan		SUV		Van	
	PMHS	GHBMC	PMHS	GHBMC	PMHS	GHBMC
Inferior Pubic Rami	0/3	No	4/5	Yes	3/3	Yes
Superior Pubic Rami	0/3	No	5/5	Yes	2/3	Yes
Iliac Wing	0/3	No	1/5	No	0/3	No
Acetabulum	0/3	No	2/5	Yes	2/3	Yes
Sacral Ala	1/3	No	3/5	Yes	2/3	Yes

Discussion

The updated GHBMC pelvis model reported biofidelic results in quasi-static SIJ loading, dynamic lateral loading, and whole-body lateral impacts while using realistic material properties. The updated model response fit in both the acetabulum loading corridors, half of the iliac wing loading corridors, all five SIJ loading corridors, and followed fracture trends seen in the whole-body impacts. This updated pelvis model is a clear improvement from the current GHBMC pelvis model (unless anterior reaction force under wing loading) and should be incorporated into future GHBMC updates.

The updated GHBMC pelvis response in dynamic lateral iliac wing loading had mixed results. The updated model reported substantially better posterior reaction results than the original GHBMC pelvis model. The original response fell outside of the corridor for the entire experiment and was below the bottom corridor by as much as 300N while the updated response laid within the corridors for the entire experiment. In contrast, the updated anterior response performed slightly worse than the original model, falling outside of the corridors for the majority of the experiment, but only by as much as 100N towards the end of the experiment. Despite the slightly worse anterior reaction response of the updated model, it is recommended to incorporate these updated material parameters.

A limitation of this pelvis model is the acetabulum cartilage model. The acetabulum cartilage geometry and thickness were not found from medical imagining, but were estimated using medical illustrations from Grey's Anatomy and reported thickness from literature [31, 32]. Due to a lack of available acetabulum cartilage research, the material properties of the cartilage were assigned to be the same as the original SIJ cartilage, a Mooney-Rivlin rubber. In a sensitivity check, these material properties were seen to have a small impact on the dynamic lateral acetabulum loading response. Future work should involve reconstructing the acetabulum cartilage from medical imagining to improve model biofidelity.

A second limitation revolves around the SIJ design. Both the original and updated GHBMC pelvis models used simplified SIJ ligaments by not including the sacrospinous and sacrotuberous ligaments which connect various portions of the sacrum to the iliac wings. These ligaments were represented in the simplified GHBMC SIJ ligaments that more closely resembled the sacroiliac ligaments. Incorporating the ignored ligaments may create a more biofiedlic response, but will increase computational cost as well. Despite the lack of these ligaments, the updated GHBMC model produced biofidelic loading and injury responses.

This updated GHBMC pelvis model had a more biofidelic response than the original GHBMC pelvis model in three validation simulations and reported realistic fracture responses in full body impacts. Future versions of the GHBMC model will incorporate these pelvis updates, and computational safety researchers should use this pelvis model as an accurate tool to predict injuries in impact scenarios.

Conclusion

Car-to-Pedestrian Collisions kill and injure thousands of pedestrians every year, and the problem is only growing in the United States. In order to improve pedestrian safety on the road, car manufacturers need proper safety investigation tools. The Global Human Body Model Consortium's male 50ᵗʰ percentile pedestrian model is a low cost and time-efficient tool for investigating pedestrian road injuries. The pelvis model updates outlined in this paper improve the biofidelity of this human model, leading to better investigations of pedestrian injury mechanics and improved pedestrian safety.

Acknowledgments

References

1. World Health Organization. *Global status report on road safety*. 2018.
2. GHSA, *Pestrian Traffic Fatalities by State*. 2018.
3. Shin, J., N. Yue, and C.D. Untaroiu, *A finite element model of the foot and ankle for automotive impact applications.* Ann Biomed Eng, 2012. **40**(12): p. 2519-31.
4. ANCAP, *ANCAP Assessment Protocol-Pedestrian Protection v9.0.2*. 2018: http://s3.amazonaws.com/cdn.ancap.com.au/app/public/assets/16b1499fb47d17738b2a5daddbbba1eff544c7cd/original.pdf?1513576121.
5. CNCAP, *CNCAP Management Regulation*. 2018: http://www.c-ncap.org/upload/201707/0318131399wr.pdf.
6. EURONCAP, *Pedestrian Testing Protocol v8.5*. 2019, Euro NCAP: https://cdn.euroncap.com/media/41769/euro-ncap-pedestrian-testing-protocol-v85.201811091256001913.pdf.
7. EURONCAP, *Pedestrian Testing Protocol*. 2017, Euro NCAP: file:///C:/Users/Student/Downloads/euro-ncap-pedestrian-testing-protocol-v84.pdf.
8. Gayzik, F., et al., *External landmark, body surface, and volume data of a mid-sized male in seated and standing postures.* Annals of biomedical engineering, 2012. **40**(9): p. 2019-2032.
9. Mao, H., et al., *Development of a finite element human head model partially validated with thirty five experimental cases.* J Biomech Eng, 2013. **135**(11): p. 111002.
10. DeWit, J.A. and D.S. Cronin, *Cervical spine segment finite element model for traumatic injury prediction.* J Mech Behav Biomed Mater, 2012. **10**: p. 138-50.
11. Li, Z., et al., *Rib Fractures Under Anterior-Posterior Dynamic Loads: Experimental and Finite-Element Study.* Journal of Biomechanics, 2010. **43**: p. 228.234.
12. Li, Z., et al., *Influence of mesh density, cortical thickness and material properties on human rib fracture prediction.* Medical engineering & physics, 2010. **32**(9): p. 998-1008.
13. Poulard, D., et al., *Thoracic response targets for a computational model: A hierarchical approach to asses the biofidelity of a 50th-percentile occupant male finite element model.* J Mech Behav Biomed Mater, 2015.
14. Soni, A. and P. Beillas, *Modelling hollow organs for impact conditions: a simplified case study.* Comput Methods Biomech Biomed Engin, 2013. **[Epub ahead of print]**.
15. Kim, Y.H., J.E. Kim, and A.W. Eberhardt, *A new cortical thickness mapping method with application to an in vivo finite element model.* Comput Methods Biomech Biomed Engin, 2012. **17**(9): p. 997-1001.

16. Shin, J. and C.D. Untaroiu, *Biomechanical and injury response of human foot and ankle under complex loading.* J Biomech Eng, 2013. **135**(10): p. 101008.

17. Untaroiu, C., et al., *A finite element model of the lower limb for simulating pedestrian impacts.* Stapp car crash journal, 2005. **49**: p. 157.

18. Yue, N. and C.D. Untaroiu, *A numerical investigation on the variation in hip injury tolerance with occupant posture during frontal collisions.* Traffic Inj Prev, 2014. **15**(5): p. 513-22.

19. Yue, N., J. Shin, and C.D. Untaroiu, *Development and Validation of an Occupant Lower Limb Finite Element Model*, in *SAE Technical Paper Series*. 2011.

20. Hayes, A.R., et al., *Validation of simulated chestband data in frontal and lateral loading using a human body finite element model.* Traffic Inj Prev, 2014. **15**(2): p. 181-6.

21. Park, G., et al., *Comparison of Kinematics of GHBMC to PMHS on the Side Impact Condition*, in *International Research Council on Biomechanics of Injury*. 2013: Gothenburg, Sweden.

22. Vavalle, N.A., et al., *Application of radial basis function methods in the development of a 95th percentile male seated fea model.* Stapp car crash journal, 2014. **58**: p. 361.

23. Vavalle, N.A., et al., *An evaluation of objective rating methods for full-body finite element model comparison to PMHS tests.* Traffic Inj prev, 2013. **14**: p. 87

24. Vavalle, N.A., et al., *Lateral impact validation of a geometrically accurate full body finite element model for blunt injury prediction.* Ann Biomed Eng, 2013. **41**(3): p. 497-512.

25. Vavalle, N.A., et al., *Investigation of the Mass Distribution of a Detailed Seated male Finite Element Model.* J. Appl Biomech, 2014. **30**(3): p. 471-6.

26. Gayzik, F.S., et al., *Development of a full body CAD dataset for computational modeling: a multi-modality approach.* Annals of biomedical engineering 2011. **39**.

27. Gordon, C., et al., *1989 Anthropometric survery of US army personnel: methods and summary statistics*. 1989, Anthropology Reserach Project Inc: Yellow Springs, OH.

28. Kemper, A., C. McNally, and S. Duma, *Dynamic tensile material properties of human pelvic cortical bone*, in *Rockey Mountain Bioengineering Symposium & International ISA Biomedical Sciences Instrumentation Symposium*. 2008: Copper Mountain, Colorado.

29. Kikuchi, Y., Y. Takahashi, and F. Mori, *Development of a Finite Element Model for a Pedestrian Pelvis and Lower Limb.* 2006.

30. Untaroiu, C., *Development and Validation of a Finite Element Model of Human Lower Limb*, in *School of Engineering and Applied Sciences*. 2005, University of Virginia.

31. Drake, R., W. Vogl, and A. Mitchell, *Grays Anatomy for Students*. 2 ed. 1904.

32. Allen, B., et al., *Acetabular Cartilage Thickness: Accuracy of Three-Dimensional Reconstructions from Multidetector CT Arthograms in a Cadaver Study.* Radiology, 2010. **255**(2).

33. Salzar, R.S., et al., *Load path distribution within the pelvic structure under lateral loading.* International Journal of Crashworthiness, 2009. **14**(1): p. 99-110.

34. Takahashi, Y., et al., *Investigation On Pedestrian Pelvis Loading Mechanisms Using Finite Element Simulations*, in *IRCOBI Conference*. 2010: Hanover, Germany.

35. Neice, R., *Development and Validation of a Pelvis Finite Element Model for Side Panel Intrustion Threats*. 2019, University of Virginia.

36. Jensen, M., et al., *LSTC Legform Impactor Finite Element Model*, Documentation_Legform_Impactor_V2.3.2, Editor. 2014, LSTC.

37. Miller, J.A., A.B. Schultz, and G.B. Andersson, *Load Displacement Behavior of Sacroiliac Joints.* Journal of Orthopaedic Research, 1987. **5**.

38. Song, E., et al. *Reference PMHS Tests to Assess Whole-Body Pedestrian Impact Using a Simplified Generic Vehicle Front-End*. in *IRCOBI Conference Proceedings*. 2017.

39. IIHS, *General statistics*. 2016: http://www.iihs.org/iihs/topics/t/general-statistics/fatalityfacts/passenger-vehicles.